ELSEVIER

Solid State Ionics 113–115 (1998) 43–49

SOLID STATE IONICS

Structural and electrical characterization of $Li(Mn_{1-\delta}Ti_{\delta})_2O_4$ electrode materials

Kwang Soo Yoo[a,*], Nam Woong Cho[b], Yong-Joo Oh[a]

[a]*Department of Materials Science and Engineering, The University of Seoul, 90 Cheonnong-dong, Tongdaemun-gu, Seoul 130-743, South Korea*

[b]*Materials Research Division, Research Institute of Industrial Science and Technology, 32 Hyoja-dong, Nam-ku, Pohang 790-330, South Korea*

Accepted 8 August 1998

Abstract

The spinel $Li(Mn_{1-\delta}Ti_{\delta})_2O_4$ electrode materials were synthesized by solid state reaction. The crystal structure by a Rietveld method and electrical properties by an impedance analyzer is characterized in the present study. The Mn_3O_4 second phase was shown in all samples. The titanium dissolved in Mn 16d-site, and the lattice constants increased and the electrical conductivity decreased with increasing titanium content. From the impedance analysis, the contribution of grain, grain boundary, and electrode was identified. Finally, the charge and discharge test was performed. © 1998 Published by Elsevier Science B.V. All rights reserved.

Keywords: Lithium manganate; Lithium secondary battery; Impedance spectroscopy; Charge–discharge test

Materials: $Li(Mn_{1-\delta}Ti_{\delta})_2O_4$

1. Introduction

Recently, the lithium-based metal oxides are being watched with interest since they began to be used as the cathode (positive electrode) materials in lithium-ion or lithium-polymer secondary batteries. More than 200 inorganic and polymer materials have been suggested for use in cathode materials of lithium secondary batteries over the past century, but now $LiCoO_2$ has been commercialized [1–3]. However, because the cobalt in $LiCoO_2$ is a rare metal, expensive and toxic, $LiNiO_2$ and $LiMn_2O_4$ are being studied as alternative materials [4,5]. The x value in $Li_xNi_{1-x}O_2$ varies 0.3–0.5 according to processing conditions and, thus, it is difficult to fabricate stoichiometric $LiNiO_2$. In the case of $LiMn_2O_4$ with spinel structure, its discharge voltage appears in the 3–4 V range and is stable near 4 V ($Li_{1-x}Mn_2O_4$, $0.15 < x < 0.75$), and its life cycle performance is not good. However, $LiMn_2O_4$ is electrochemically and thermally stable except for its economical and environmental advantages. The reason is that $LiMn_2O_4$ has only Li-deserted λ-MnO_2 structure (Eq. (1)) but in the case of $LiCoO_2$ and $LiNiO_2$ the inner pressure of batteries increases due to oxygen

*Corresponding author. Tel.: +82-2-2102514; fax: +82-2-2491441; e-mail: ksyoo@uoscc.uos.ac.kr

0167-2738/98/$ – see front matter © 1998 Published by Elsevier Science B.V. All rights reserved.
PII: S0167-2738(98)00365-8

occurring by irreversible reaction when overcharged (Eqs. (2) and (3)) [6].

$$LiMn_2O_4 \xrightarrow[-e^-]{-Li^+} 2MnO_2 \quad (1)$$

$$LiCoO_2 \xrightarrow[-e^-]{-Li^+} \frac{1}{3}Co_2O_3 + \frac{1}{3}CoO + \frac{1}{3}O_2(g) \quad (2)$$

$$LiNiO_2 \xrightarrow[-e^-]{-Li^+} NiO + \frac{1}{2}O_2(g) \quad (3)$$

To improve the cycle performance of $LiMn_2O_4$, the addition of excess lithium [7], the change of preparation conditions such as firing temperature and oxygen atmosphere [8], the substitution of some elements for Mn [9], etc. have been studied by several investigators.

Accordingly, the objective of the present study is to synthesize the $Li(Mn_{1-\delta}Ti_\delta)_2O_4$ materials by substitutionally doping manganese with titanium, analyze their crystal structures and electrical properties and, thus, provide the basic information for use in cathode materials of lithium secondary batteries. The specimens were prepared by typical ceramic powder processing, the crystal structures were extensively analyzed by the Rietvelt method to X-ray powder diffraction data, and finally the impedance analyses and charge-discharge tests were performed.

2. Experimental

A tentative substitution of a large amount of manganese with titanium ($Li(Mn_{1-\delta}Ti_\delta)_2O_4$ with $0 \leq \delta \leq 0.2$) was carried out using a typical ceramic powder processing. The raw materials used are as follows: Li_2CO_3 (99.9%, High Purity Chemical), MnO_2 (99.9%, CERAC), and TiO_2 (99.9%, CERAC). Powders of each specimen were weighed by the required composition, mechanically mixed and milled using a ball mill for 24 h and then calcined at 800°C for 24 h. The calcined powders added with 1 wt.% polyethylene glycol were ground using an agate mortar and pressed into pellets under a pressure of 700 kg/cm^2. These samples were then fired at 850 and 1100°C for 4 h in air, respectively.

The analysis of the crystal structure of $Li(Mn_{1-\delta}Ti_\delta)_2O_4$ were carried out by a powder X-ray diffractometer using Cu Kα (1.5414 Å) radiation (RINT, Rigaku). The powder samples were prepared by grinding to under 10 μm in particle size using an agate mortar. The measurement range was 10–80° and the step scan was 0.02°. The phase identification and the evaluation of lattice parameter for the measured data were refined using cell program, and the Rietveld profile analysis on the measured X-ray diffraction (XRD) patterns was then performed using the RIETAN program by Izumi [10].

The electrical properties were measured at room temperature using a computer-controlled impedance analyzer (Impedance/Gain Phase Analyzer, Model No. 1260, Solatron) in the frequency range of 0.1 Hz–20 MHz. For the electrical measurements, two parallel faces of pellets were polished, painted with Pt/Ag paste (Tanaka Noble Metal International), and fired at 850°C for 12 min for good electrical contacts. To investigate electrode effects, the Ag paste (Dotite, D-550, Fugikura Kasei) with relatively high resistance was painted to the same pellets at room temperature. The size of the pellets was approximately 13 mm in diameter and 1.0 mm in thickness.

Finally, the electrochemical properties were evaluated with a 2-h step using a half cell. The cell consists of $Li(Mn_{1-\delta}Ti_\delta)_2O_4$ as a cathode, a lithium metal foil as an anode, and a lithium as a reference, and 1 M $LiClO_4$ dissolved in propylene carbonate solution as an electrolyte. The cathode was prepared by mixing the active material, $Li(Mn_{1-\delta}Ti_\delta)_2O_4$, with acetylenized carbon black and a binder made from polyvinylidene fluoride (PVDF) and *N*-methyl-2-pyrrolidone (NMP) solution.

3. Results and discussion

3.1. X-ray diffraction analysis

The crystal structure of $LiMn_2O_4$ is the spinel as shown in Fig. 1 and its space group is Fd3m (cubic, no. 227). The spinel structure is of an oxygen cubic close-packed (ccp) type and the cubic unit cell of twice of the lattice parameter of this ccp structure is an ideal unit cell of the spinel structure. This unit cell contains 32 oxygens (32e-site of the Fd3m space group). The lithiums occupy one-eighth of 64 tetra-

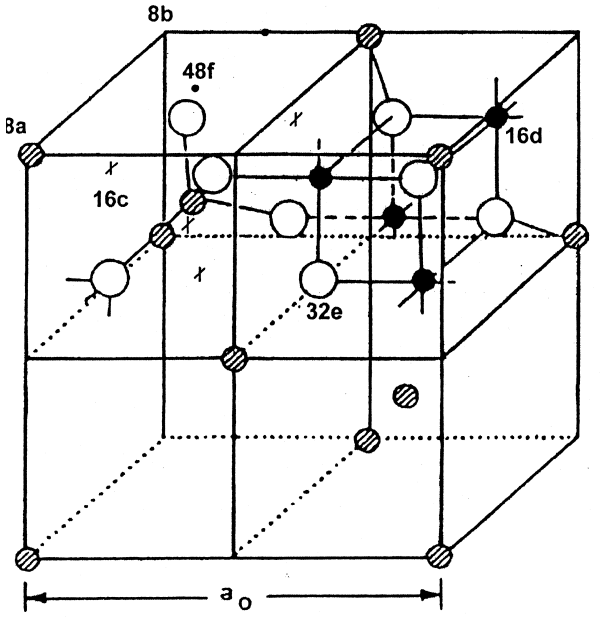

Li : 8*a* $0,0,0\ ;\ \frac{1}{4},\frac{1}{4},\frac{1}{4}$

Mn : 16*d* $\frac{5}{8},\frac{5}{8},\frac{5}{8}\ ;\ \frac{5}{8},\frac{7}{8},\frac{7}{8}\ ;\ \frac{7}{8},\frac{5}{8},\frac{7}{8}\ ;\ \frac{7}{8},\frac{7}{8},\frac{5}{8}$

O : 32*e* $x,x,x\ ;\ \frac{1}{4}-x,\frac{1}{4}-x,\frac{1}{4}-x\ ;\ x,\bar{x},\bar{x}\ ;\ \frac{1}{4}-x,\ \frac{1}{4}+x,\frac{1}{4}+x\ ;\bar{x},x,\bar{x}\ ;\ \frac{1}{4}+x,\frac{1}{4}-x,\frac{1}{4}+x\ ;\ \bar{x},\bar{x},x\ ;\ \frac{1}{4}+x,\frac{1}{4}+x,\frac{1}{4}-x$

Fig. 1. Schematic diagram of the $LiMn_2O_4$ spinel structure.

hedral sites (8a) and the manganeses occupy half of 32 octahedral sites (16d). In addition, there are vacancies in 16c octahedral and 8b and 48f tetrahedral sites. The 16c octahedral sites share faces with 8a and 48f tetrahedral sites to provide a continuously interconnected interstitial space through which lithium can reversibly be incorporated into the structure [11,12].

As shown in Fig. 2, the spinel $Li(Mn_{1-\delta}Ti_{\delta})_2O_4$ materials can be synthesized at 850°C by solid state reaction. With increasing titanium content, their

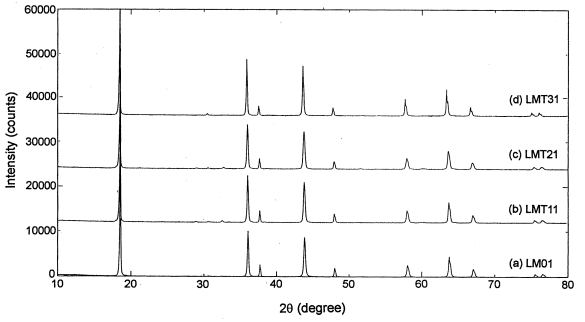

Fig. 2. Powder X-ray diffraction patterns of $Li(Mn_{1-\delta}Ti_{\delta})_2O_4$ fired at 850°C: (a) $LiMn_2O_4$; (b) $Li(Mn_{0.95}Ti_{0.05})_2O_4$; (c) $Li(Mn_{0.90}Ti_{0.10})_2O_4$; and (d) $Li(Mn_{0.80}Ti_{0.20})_2O_4$.

diffraction patterns are the same as that of $LiMn_2O_4$ and the same phase was identified. Table 1 gives the results of Rietveld refinements for XRD data of $Li(Mn_{1-\delta}Ti_{\delta})_2O_4$. Fig. 3 shows the measured XRD pattern, the calculated pattern, and their difference for the sample LMT21 ($Li(Mn_{0.9}Ti_{0.1})_2O_4$). The level of agreement between the measured pattern and the fitted pattern is indicative of a reliable refinement. The other samples also gave equally good fits. It was confirmed that the Mn_3O_4 second phase as shown in Fig. 3 exists in all samples.

At this time, it was identified that the titanium dissolved in Mn 16d-site (5/8, 5/8, 5/8). As the results of the calculated *R* factors in Rietveld refinements as shown in Table 1, the *R* values were lower when the titanium is located in the 16d-site than other sites. The structural analysis results in $S=2.58–3.50\%$, $R_I=2.92–5.03\%$ and $R_F=2.16–4.44\%$. The *S* (goodness of fit), R_I (integrated intensity factor), and R_F (structure factor) values show the degree of agreement between the values measured by an X-ray diffractometer and calculated by a model structure. In other words, these factors indicate how well the peak intensities are reproduced. These values were calculated as follows:

Table 1
The results of Rietveld refinements of X-ray diffraction data for $Li(Mn_{1-\delta}Ti_{\delta})_2O_4$

Sample	Composition	Firing temperature (°C)	Lattice parameter (Å)	x[a]	S[b]	R factor (%)	
						R_I[c]	R_F[d]
LM01	$LiMn_2O_4$	850	8.2363	0.3876	2.74	2.92	2.16
LM02	$LiMn_2O_4$	1100	8.2383	0.3859	2.70	2.98	3.15
LMT11	$Li(Mn_{0.95}Ti_{0.05})_2O_4$	850	8.2459	0.3882	3.50	5.03	4.43
LMT12	$Li(Mn_{0.95}Ti_{0.05})_2O_4$	1100	8.2507	0.3876	2.81	3.69	3.12
LMT21	$Li(Mn_{0.90}Ti_{0.10})_2O_4$	850	8.2522	0.3885	3.46	5.31	4.44
LMT22	$Li(Mn_{0.90}Ti_{0.10})_2O_4$	1100	8.2623	0.3884	2.79	3.19	2.73
LMT31	$Li(Mn_{0.80}Ti_{0.20})_2O_4$	850	8.2860	0.3890	2.83	4.82	3.85
LMT32	$Li(Mn_{0.80}Ti_{0.20})_2O_4$	1100	8.2881	0.3884	2.58	3.09	2.52

[a]Coordinate of 32e-site in AB_2O_4 spinel structure.
[b]Goodness of fit.
[c]Intergrated intensity R factor.
[d]Structure R factor.

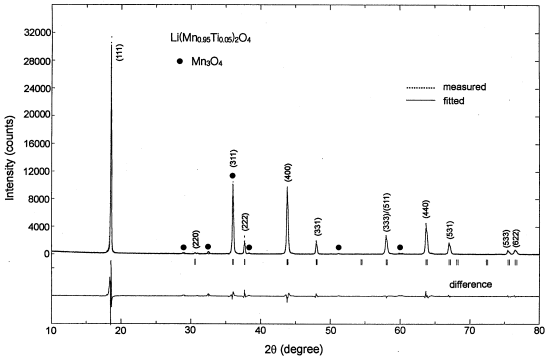

Fig. 3. Powder X-ray diffraction patterns of $Li(Mn_{0.95}Ti_{0.05})_2O_4$ fired at 850°C. The dots represent the measured intensities and the solid line the fitted ones. The difference curve between the measured curve and the fitted one is shown beneath.

$$S = R_{wp}/R_e, R_e = [(N-P)/\sum w_i y_i]^{1/2} \quad (4)$$

$$R_I = \sum |I_o - I_c| / \Sigma I_o \quad (5)$$

$$R_F = \sum |I_o^{1/2} - I_c^{1/2}| / \sum I_o, \quad (6)$$

where I_o is the observed integrated intensity and I_c is calculated one, and P and N are the number of measured data and parameter used in calculation, respectively. In the calculation process, zero point, background, and asymmetry parameters were corrected. With increasing δ in $Li(Mn_{1-\delta}Ti_{\delta})_2O_4$, the coordinate of the O 32e-site, x, was not significantly different.

As shown in Table 1 and Fig. 4, the lattice

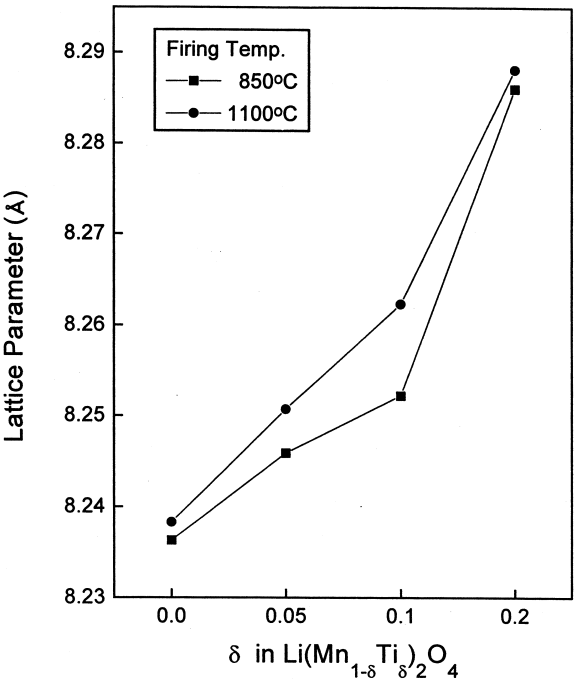

Fig. 4. Lattice constants of $Li(Mn_{1-\delta}Ti_{\delta})_2O_4$ obtained from Rietveld refinements.

constant increases because the diffraction peaks shift to low angles with increasing δ value in $Li(Mn_{1-\delta}Ti_{\delta})_2O_4$. These results accord with the difference of ionic radii between Mn^{4+} (0.053 nm) and Ti^{4+} (0.061 nm) in the octahedral site [13]. For the same composition, it was shown that the lattice parameter prepared at high temperature is greater.

3.2. Impedance analysis

Impedance measurements were taken to identify the roles of the grain (interior) and grain boundary in the $Li(Mn_{1-\delta}Ti_{\delta})_2O_4$ materials and the change of impedance spectra with increasing δ value.

Fig. 5a shows the complex impedance spectra of the sample LMT12 ($Li(Mn_{0.95}Ti_{0.05})_2O_4$) obtained at room temperature in air. How the response is separated into contributions from grain, grain boundary, and electrode is indicated in Fig. 5a. Fig. 5a shows that the resistance of the sample (grain and grain boundary) is approximately 240 Ω for the same sample, $Li(Mn_{0.95}Ti_{0.05})_2O_4$, and different elec-

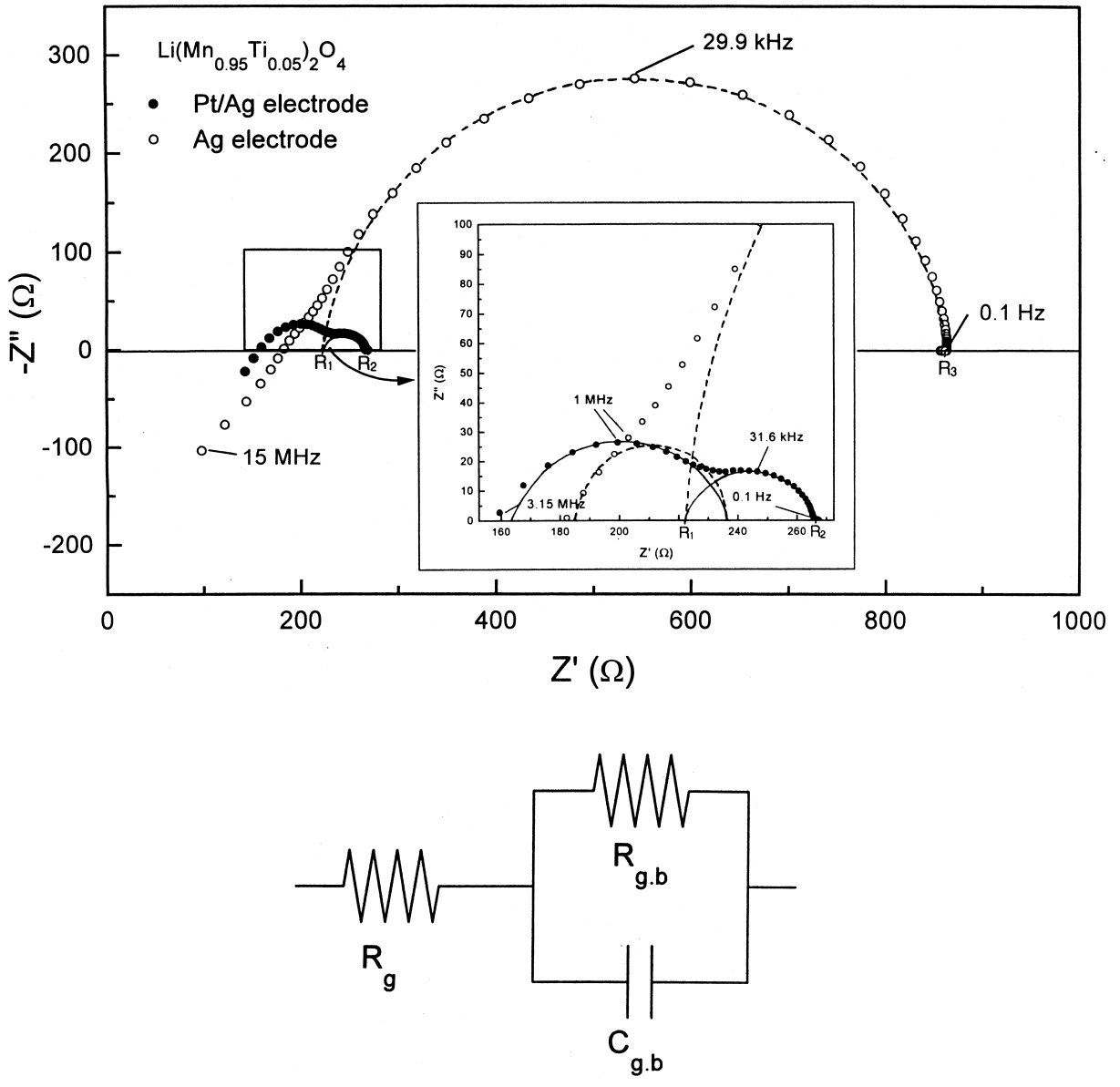

Fig. 5. (a) Complex impedance spectra of $Li(Mn_{0.95}Ti_{0.05})_2O_4$ obtained at room temperature and (b) an equivalent circuit of $Li(Mn_{0.95}Ti_{0.05})_2O_4$.

trodes. However, the right semicircle of each spectrum in the low-frequency range shows that the electrode resistances are greatly different as follows: 44 and 638 Ω (R_2-R_1 and R_3-R_1 in Fig. 5a) for Pt/Ag fired at 850°C and Ag painted at room temperature, respectively. The Ag electrode was used to confirm no change of the sample resistance. A simplified equivalent circuit for this sample which was used to fit the measured impedance data is shown in Fig. 5b. The program used for the equivalent circuit plotting and impedance calculation was ZView Equivalent Circuits [14]. Table 2 shows grain resistance (R_g), grain boundary resistance (R_{gb}), and grain boundary capacitance (C_{gb}) calculated by ZView program. As a result of the ZView fitting, the R_g and R_{gb} values for each sample are within the error range of 5% and different from those obtained from the semicircles of each spectrum (R_a, R_b and R_c in Fig. 6). With increasing titanium content, both the resistances of grain and grain boundary tend to increase and the electrical conductivities decreased from 2.6×10^{-4} to 1.9×10^{-4} Ω^{-1} cm^{-1}.

As shown in Fig. 6, for each sample, the left semicircle in the high-frequency range shows the effect of grain boundaries and may show the effect of the porosity. With increasing titanium content, the grain boundaries increased with decreasing the grain size. It was reported that the semicircle for grain boundaries was enlarged by the porosity, while maintaining its shape [15]. In this case, it is assumed that the reason which the resistance of grain boundary is large is due to some pores in the sample.

3.3. Charge–discharge test

Fig. 7 compares the charge and discharge characteristics of $Li(Mn_{1-\delta}Ti_{\delta})_2O_4$. In this test, the cathode materials were prepared at 1100°C, which are the same as the materials used for impedance analysis. In Fig. 7a–d, the charge capacities were 107.5, 77.0, 84.6 and 57.7 mAh/g, respectively, and the potential plateau for discharge was 3.7 V.

4. Summary

The spinel $Li(Mn_{1-\delta}Ti_{\delta})_2O_4$ electrode materials were synthesized by solid state reaction. The Mn_3O_4 second phase was shown in all samples. As a result of Rietveld refinements, the titanium dissolved in Mn

Table 2
The results of the impedance spectra of $Li(Mn_{1-\delta}Ti_{\delta})_2O_4$ fitted by ZView program

Composition	R_g (Ω)	R_{gb} (Ω)	C_{gb} (F)	R^a_{sample} (Ω)	σ^b_{sample} ($\Omega^{-1}\cdot cm^{-1}$)
$Li(Mn_{0.95}Ti_{0.05})_2O_4$	176.8	85.2	5.17×10^{-9}	262.0	2.7×10^{-4}
$Li(Mn_{0.90}Ti_{0.10})_2O_4$	203.7	160.4	3.21×10^{-8}	364.1	2.0×10^{-4}
$Li(Mn_{0.80}Ti_{0.20})_2O_4$	404.7	234.9	5.13×10^{-10}	639.6	1.9×10^{-4}

[a] $R_{sample}=R_g+R_{gb}$.
[b] $\sigma_{sample}=(d)/(R_{sample}\cdot A)$ (A, electrode area; d, thickness of the sample).

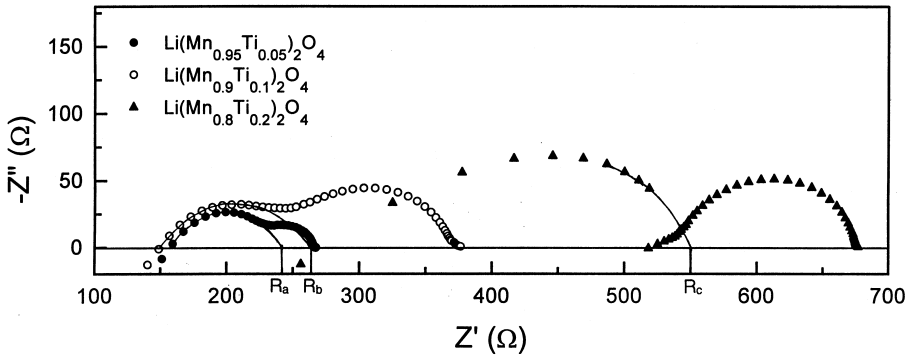

Fig. 6. Complex impedance spectra of $Li(Mn_{1-\delta}Ti_{\delta})_2O_4$ obtained at room temperature using Pt/Ag electrode.

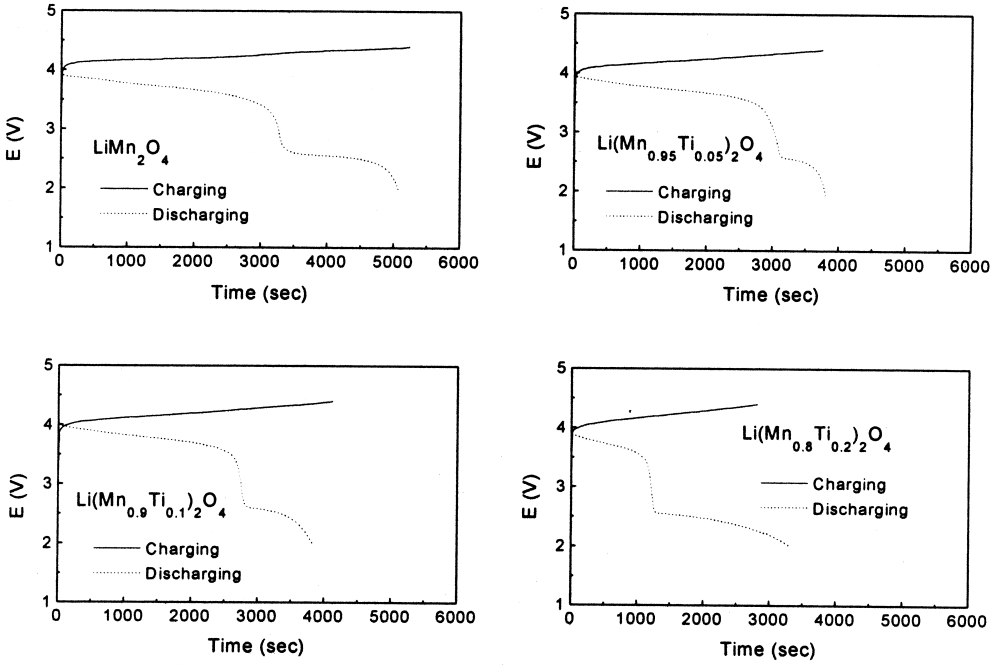

Fig. 7. Charge–discharge curves of $Li(Mn_{1-\delta}Ti_{\delta})_2O_4$ ($\delta=0$, 0.05, 0.1, 0.2) prepared at 1100°C.

16d-site and the lattice constants increased with increasing the titanium content. The structural analysis resulted in $S=2.58$–3.50%, $R_I=2.92$–5.03% and $R_F=2.16$–4.44% and, thus, the fitted patterns were in good agreement with the measured patterns. The results of impedance analyses show that the resistances of grain and grain boundary increased and the electrical conductivity decreased from 2.6×10^{-4} to 1.9×10^{-4} Ω^{-1} cm^{-1} with increasing titanium content. The resistances of grain boundaries are 85–235 Ω and it is assumed that these large values are due to the pore effect. The potential plateau for discharge was 3.7 V.

References

[1] M.M. Thackeray, J. Electrochem. Soc. 142 (1995) 2558.
[2] V. Menev, A. Momchilov, A. Kozawa, in: Progress in Batteries and Battery Materials, vol. 14, ITE-JEC Press Inc., Japan, 1995, p. 102.
[3] K.M. Abraham, Electrochem. Acta 38 (1993) 1233.
[4] A. Hirano, R. Kanno, Y. Kawamoto, K. Oikawa, T. Kamiyama, F. Izumi, Solid State Ionics 86–88 (1996) 791.
[5] A. Yamada, K. Miura, K. Hinokuma, M. Tanaka, J. Electrochem. Soc. 142 (1995) 2149.
[6] C.-H. Doh, in: 1st Symposium on the Lithium Secondary Batteries, Center for Interface Sci. & Eng. of Materials, Korea Advanced Institute of Science and Technology, Taejon, Korea, 1997, p. 13.
[7] R.J. Gummow, A. de Kock, M.M. Thackeray, Solid State Ionics 69 (1994) 59.
[8] Y. Gao, J.R. Dahn, J. Electrochem. Soc. 143 (1996) 100.
[9] L. Guohua, H. Ikuta, T. Uchida, M. Wakihara, J. Electrochem. Soc. 143 (1996) 178.
[10] F. Izumi, in: R.A. Young (Ed.), The Rietveld Method, ch. 13, Oxford University Press, Oxford, 1993.
[11] C. Giacovazzo, in: Fundamentals of Crystallography, Oxford University Press, Oxford, 1994, p. 442.
[12] N. Kumagai, T. Fujiwara, K. Tanno, T. Horiba, J. Electrochem. Soc. 143 (1996) 1007.
[13] Y.-M. Chiang, D.B. Birnie, W.D. Kingery, in: Physical Ceramics, John Wiley & Sons, Inc., New York, 1997, p. 15.
[14] ZView for Windows, Impedance/Gain Phase Graphing and Analysis Software, Operating Manual version 1.4, Scribner Associates, Inc., Charlottesville, 1996, p. 7.1.
[15] A.D. Brailsford, D.K. Hohnke, Solid State Ionics 11 (1983) 133.